Cryobiology 111 (2023) 1–8

Contents lists available at ScienceDirect

Cryobiology

journal homepage: www.elsevier.com/locate/cryo

A novel automated protocol for ice crystal segmentation analysis using Cellpose and Fiji

Joshua Saad, Madison Fomich, Vermont P. Día, Tong Wang *

Department of Food Science, The University of Tennessee, 2510 River Drive, Knoxville, TN, 37996-4539, USA

ARTICLE INFO

Keywords:
Image analysis
Automation
Cellpose
Masking
Ice crystal size and shape

ABSTRACT

Accurate measurement of ice crystal size is an essential step in quantitative ice recrystallization inhibition (IRI) analysis using the sucrose sandwiching assay (SSA) and splat assay (SA). Here, we introduce a novel method of measuring ice crystal size and shape using Fiji and Cellpose, an anatomical segmentation algorithm, to address the time-consuming and limited number of ice particle determination associated with the mean largest grain size measurement. This new automated approach, displaying rapid segmentation of ~70 s per image, measures every ice crystal in an image field of view, consequently reducing bias introduced by subjectively selecting the largest crystals in an image. Consistent in determining a diverse set of crystal sizes and shapes, this method allows for the evaluation of ice crystals using Feret's diameter, a parameter that better accounts for irregular particle shape. This method provides new outputs such as standard deviation, particle size distributions of a population of ice crystals, and circularity to characterize and further provide insight into an analyte's IRI ability. Applicable to the SSA, the "shape descriptor" measurement can be used to quantify ice binding. This work presents a novel and accurate approach for ice crystal quantitative analysis.

1. Introduction

Accurate ice crystal size and shape quantification is essential for evaluating ice recrystallization inhibition (IRI) activity, commonly performed using the splat assay (SA) and sucrose sandwiching assay (SSA) [1]. The output from these assays provides similar parameters in which ice crystals are evaluated: the SSA allows viewing of crystal shape influenced by analyte interaction on a particular binding plane of the ice, additionally allowing quantification of ice crystal size, while the SA measures capability of the analyte to suppress ice growth, evaluating reduction of ice crystal size [1,5,14]. Quantification of ice crystal size and shape is paramount in assessing the results obtained by these procedures. While both methods rely on quantitative ability, the SA proves challenging because of the numerous crystals whose borders meet, while the SSA is less cumbersome to analyze due to its lower abundance of crystals and increased spacing. Current determination of analyte ice binding within a particular crystal plane is largely qualitative, lacking quantification methods of ice crystal shape determination. Data analysis of the SA can be time-consuming due to the large number of ice crystals generated, and it will only provide meaningful output if a significant number of crystals are measured.

For the conventional SA method, a measurement known as the mean largest grain size (MLGS) has been the most used parameter reported in literature. This measurement is often for the ten largest ice crystals in a field of view (FOV) measured by the diameter of a consistent angle or ellipsis [2]. The MLGS measurement is limited in its characterization of ice crystal size and shape, as it lacks the ability to analyze all crystals present in a FOV, only measuring a limited number of ice crystals in both the sample and control to compare size. Lacking automated programming, population analysis of ice crystals in a FOV is labor intensive. Manual measurement and calculation with the assistance of programs such as Fiji can increase efficiency, but regardless the method is slow in generating quantitative output, as it still requires manual measurement and determination of the largest crystals. This MLGS measurement presents many limitations in how these results are interpreted, warranting further development of an improved method for analyzing ice crystal size and shape. If every crystal in a FOV was subject to measurement, a particle size distribution could be generated and compared

Abbreviations: FD, Feret or Feret's diameter; FOV, field of view; IRI, ice recrystallization inhibition; MLGS, mean largest grain size; MGS, mean grain size; PVA, polyvinyl alcohol; ROI, region of interest; SA, splat assay; SSA, sucrose sandwiching assay; PEG, polyethylene glycol.

* Corresponding author.
E-mail address: twang46@utk.edu (T. Wang).

https://doi.org/10.1016/j.cryobiol.2023.02.002
Received 12 September 2022; Received in revised form 2 February 2023; Accepted 6 February 2023
Available online 10 February 2023

against different treatments and conditions to further characterize the ice crystal population. This ideal analysis model would not bias the measurement based on shape, is sensitive to particle size distribution, and would provide other parameters such as shape descriptors and standard deviations for population size and shape. Similar concerns were identified and rectified through the creation of Cellpose, capable of masking (i.e. identify and mark a particle) every cell in an image FOV in an automated manner [13].

Cellpose is a deep learning-based segmentation program originally designed for segmentating cells and cell parts [13]. The program has been implemented for segmentation of stained skeletal muscle fibers and for other biological applications, achieving success in accurate and descriptive segmentation [9,15]. Cellpose works by using generated topographical maps predicted by a neural network to stipulate if a pixel is inside a region of interest (ROI). Utilizing gradient tracking, all pixels in a given cell can be identified by a center point and thus the shape of the cell can be determined and masked, further articulated by the program's neural network removing pixels outside the ROI boundaries [13]. Because of the similarities between snap-frozen cross-section skeletal muscle fiber structure viewed under a microscope, and ice crystal structure photographed during the SA and SSA, Cellpose was proposed to segment ice crystals generated by these assays quickly and accurately.

Largely automated using programs including Fiji, LabelstoROIs (Fiji plugin), and Cellpose, swift segmentation of hundreds of ice crystals per FOV in multiple images can be speedily masked and extrapolated into quantitative data far more efficiently than demarcating the ten largest crystals in the same images. Utilizing this automated method for ice crystal size and shape determination, a more statistically sound output is produced compared to the MLGS, as Cellpose masks entire populations of ice crystals present in a FOV. This output when measured by Feret's diameter (FD), a common parameter for particle size analysis that has been previously implemented for IRI analysis [11], provides superior quantification of ice crystals [16]. The goal of this work was to demonstrate the use of Cellpose, Fiji, and LabelstoROIs in automated segmentation and quantification of ice crystal size and shape, and to compare speed and quantitative ability against the conventional method reported in literature.

2. Materials and methods

2.1. Materials

Polyethylene glycol 400 (PEG, MW 380–420 Da) was purchased from TCI (Portland, OR) and polyvinyl alcohol (PVA, MW 89–98 kDa) was purchased from Sigma Aldrich (Saint Louis, MO). Peptides 1–3 were products of enzymatic hydrolysis of three food proteins produced in our laboratory, and these are mixtures of peptides of different chain lengths. Similar preparation of food protein hydrolysates for IRI was reported by Damodaran [6].

2.2. Splat assay (SA)

A standard procedure was used to analyze IRI activity of a few peptide samples. SA [7,8] was performed using 4% w/w (40 mg/mL) solutions of the peptide samples in 1x PBS buffer. One drop was delivered from 1.5-m height on to a precooled (−80 °C) microscope slide. The slide was annealed at −8 °C using a cryo-stage HCS 302 (Instec Instruments, Boulder, CO) for 30 min, with pictures taken using light microscopy (Leica, DM2700 M, Wetzlar, Germany) with a built-in digital camera (Leica, DMC 4500, Wetzlar, Germany) after 30 min.

2.3. Generation of sucrose sandwiching assay (SSA) like ice crystals

A modified SSA procedure [10] was used for the purpose of this study to allow the annealing of individual crystals to test the ability of Cellpose to segment crystals that are spread across an FOV. PEG was added to a 25% sucrose solution to create samples that were 4% (40 mg/mL) PEG. Each sample (5 μL) was placed on a glass microscope slide and covered with a cover slip (1 mm thickness, 22 × 22 mm). The sample was then placed in an Instec cold stage model TS102 (Instec Instruments, Boulder, CO) and cooled to −25 °C at a rate of 10 °C/min and annealed for 5 min until fully solid. The sample was then slowly thawed at a rate of 1 °C/min to −4 or −5 °C depending on the sample and annealed until a small number of individual crystals remained. Temperature manipulation was implemented to create well separated individual crystals solely for the purpose of evaluating the Cellpose segmentation. All temperatures were regulated using liquid nitrogen by an Instec liquid nitrogen pump and mk2000 temperature controller (Instec Instruments, Boulder, CO). Pictures were taken using light microscopy with a built-in digital camera as stated earlier after 30 min.

2.4. Calculation of the mean largest grain size (MLGS)

The MLGS was calculated by measuring the 10 largest ice crystals in each image taken during the SA using Fiji software. A single MLGS value for ice crystals in a FOV was calculated taking the sum of the 10 largest crystals in the FOV and dividing by 10. Each sample was analyzed 2 times (2 slides) and 5 FOVs were captured from each slide from which the ice crystal MLGS sizes were averaged. The average of the 5 images was then averaged between the two slides to give a single MLGS ice crystal size per sample. The time needed for assessing each FOV was recorded.

2.5. New automated analysis using Cellpose

Data was collected and analyzed using a Dell Precision 3640 Tower, Intel® Core™ i7-10700 CPU @ 2.90 GHz, 2904Mhz 8 core processor, 16.0 GB of RAM, Intel ® UHD Graphics 630, operating in Windows 10 OS. Captured images of ice crystal FOVs were imported in bulk into Cellpose (utilizing Anaconda PowerShell). Cellpose determined the vertical and horizontal gradients of each ice crystal, forming vector fields via gradient tracking. In doing so, Cellpose groups pixels from a center point to mask the irregular shapes of the ice crystals. To ensure the highest degree of accuracy in the formation of these vector fields, prior to masking, the crystal diameter was entered as zero (0) to force Cellpose to calculate the average crystal diameter from each individual ice crystal FOV. No other settings in Cellpose were adjusted with the exception of the diameter value. Upon completion, the newly masked images were exported as .png files to allow bulk data extraction in Fiji. Using a bulk renaming tool for the files, the newly generated masked .png files were then named the same name as the original images, adding "_label" to the end of the file name. This allows the LabelstoROIs plug-in to identify the corresponding masked images and original images to allow bulk quantification of the masked images. Using the LabelstoROIs plug-in in Fiji, the original images and newly named masked images were imported in bulk into LabelstoROIs and pixel erosion was set to a value of zero (0), because the initial Cellpose outlines generally reflect the crystal boundaries without the need for erosion. Measurement parameters included FD and shape descriptors. Corresponding Microsoft Excel® files containing the selected measurements were then generated and used to obtain the mean FD and standard deviation of each individual image. For the SSA samples, the mean shape descriptor value and standard deviation was calculated using Microsoft Excel®. The image boundaries were then inspected manually to verify the accuracy of the domain recognition ability of Cellpose. To keep the results unbiased, misidentified crystals were not removed from the images for the purpose of this study.

2.6. Statistical analysis

To compare the averages of the MLGS and FD calculated by Cellpose, JMP was used, and a Tukey test was performed to compare the two

methods of measuring ice crystals at a 5% probability level.

The standard deviation when referencing single images was calculated using the diameter of every individual crystal present in one image FOV. The standard deviation when referencing multiple images was calculated treating 5 images on one slide as a single observation, then the two observations from the two slides were averaged and the standard deviation was obtained.

2.7. Comparison of MLGS and Cellpose ice crystal size

Comparison of the ice crystal FOV's using the MLGS and Cellpose method were made in two different ways. First, as shown in Table 1, the heading of multiple images for MLGS and FD is the average of the two slides for each analyte, in which 5 FOV's from each slide were averaged to give a single analyte measurement value. For the MLGS, this was the 10 largest crystals in each FOV; for FD, this was a population measurement of the ice crystals present in the FOV. Thus, the standard deviation values represent the difference between the two slides. The heading of single image represents a singular FOV for each peptide sample in which the MLGS value is the average of the 10 largest crystals and FD is the value of the average of all the ice crystals present in the FOV. Here, the standard deviation represents the difference among the 10 largest crystals in the MLGS measurement or size variation among all of the ice crystals for the FD value under a single FOV.

3. Results and discussion

3.1. MLGS vs Cellpose measurement in the comparison of three peptides IRI characteristics

Comparison of ice crystal size between multiple images of two different peptide treatments, evaluated using both the MLGS and Cellpose methods, indicated large differences in mean diameter. Fig. 1a shows peptide 1 produced an FOV displaying varying crystal size and shape, with a large percentage of the image dominated by smaller crystals while large crystals manifest sporadically. Upon quantification of peptide 1, significant difference in mean crystal size was obtained between the MLGS and Cellpose methods, as shown in Table 1. This difference in crystal diameter is likely attributed to inconsistency of ice crystal sizes within the FOV, as only the large crystals are considered by the MLGS, biasing the crystal size measurement. Upon evaluation of peptide 2 (Fig. 1c), the ice crystal size present in the FOV is far more consistent when compared to peptide 1. Considering such, the MLGS measurement of peptide 1 is problematic to compare to peptide 2, as it fails to provide an accurate description of the varying crystal sizes within the FOV, when compared to the more uniform sample produced by peptide 2. As a result, the MLGS seemingly indicates that the larger average crystal size is produced by peptide 1 compared to peptide 2. This method failed to account for the sample in a holistic manner, ignoring the superior ability of peptide 1 to reduce crystal size, thus overlooking peptide 1's enhanced IRI activity when compared to peptide 2. Utilizing Cellpose and Fiji to determine the FD of the crystals, the crystal size influenced by peptide 1 is much lower than the mean diameter calculated by the MLGS. The ability of Cellpose to evaluate every crystal in the FOV provides a more accurate description of peptides 1's ability to reduce ice crystal size, allowing Cellpose's measurement to serve as a better indicator of IRI activity. This enhanced measurement of crystal size across the entire FOV changes the outcome of comparison between peptide 1 and 2, as peptide 1 displays an apparent lower FD value when compared to peptide 2, contrary to the MLGS results.

Similarly, evaluation of ice crystal size within a single image using both the MLGS and Cellpose methods displayed large differences in mean diameter. As discussed previously, the MLGS measurement is only capable of characterizing a FOV holistically if the crystal size is uniform. Upon measurement of ice crystals produced by peptide 3, shown in Fig. 2 and Table 1, the size quantified by the two methods varied greatly resulting from the MLGS selection of largest crystals compared to Cellpose's population analysis. Additionally, when using Cellpose to determine ice crystal size, the measurement of all crystals in the FOV can provide further insight into the analytes' IRI ability when evaluating the standard deviation of the crystal sizes. The large standard deviation value of peptide 3 by Cellpose reveals its varied crystal sizes within the FOV. This new quantification of ice crystal size distribution by measurement of population standard deviation by Cellpose reveals the sample's inability to control crystal size uniformity, likely unable to slow the Ostwald ripening process. When evaluated together with the mean crystal size, the user can understand not only the basic IRI activity of an analyte, but also how uniformly it is able to suppress ice growth or slow the Ostwald ripening process, allowing visualization of IRI capability without the need of an image. Though the standard deviation of the 10 largest crystals can be calculated, as seen in Table 1, it is not the same as the population standard deviation provided using Cellpose. The two measurements evaluate fundamentally different aspects of size consistency, as the MLGS only measures the consistency of the largest crystals, biasing the measurement through selection of similarly sized crystals, making comparisons between the standard deviations less useful.

Because the MLGS measurement does not take into account the entire FOV's ice crystals, biasing the size measurement toward the largest crystals, that if all the crystals in the FOV were similarly sized (in this case the MLGS would not suffer from the biasing issue), the Cellpose data is more statistically robust when compared to the MLGS measurement due to the entire ice crystal population being measured in the FOV. When referencing statistical ability, we only use it as a general term to discuss the ability to detect a true effect if present, due to the large number of ice crystals measured.

3.2. Ability of Cellpose to accurately mask a diverse set of crystal sizes and shapes

Resulting from the diverse and numerous images employed during the training of Cellpose, a wide range of crystal shapes and sizes can be evaluated. All crystals present in our study induced by different analytes and conditions could be accurately masked, seen in **Figures 1, 2, 3** (rod shaped, excluding **3c**), **4** (light intensity), and **5** (by SSA). These include

Table 1
Comparison of 3 peptide samples in inhibiting ice crystal growth measured by the standard mean largest grain size (μm) and the new procedure using Feret's maximum diameter (FD) (μm).

Sample	MLGS (Multiple images)	FD (Multiple images)	MLGS (Single image)	FD (Single image)	Circularity (Single image)	Number of crystals identified in FOV (Single image)
Peptide 1	30.7 ± 1.2^{a}	21.6 ± 0.6^{b}	28.9 ± 2.8	20.8 ± 6.5	0.80 ± 0.08	1007
Peptide 2	29.5 ± 2.0^{a}	24.2 ± 2.4^{b}	31.8 ± 4.6	30.2 ± 8.6	0.74 ± 0.08	589
Peptide 3	–	–	70.4 ± 9.6	38.4 ± 16.7	0.78 ± 0.08	261

4% PEG had a MLGS 58.3 ± 2.9 (multiple images) and a FD of 48.4 ± 1.0 (multiple images). "–" indicates that data was not collected. Means with different superscripts within "multiple images" and in the same row are significantly different ($P < 0.05$). The standard deviation for any single image measurement is the variation of crystal size under one image.

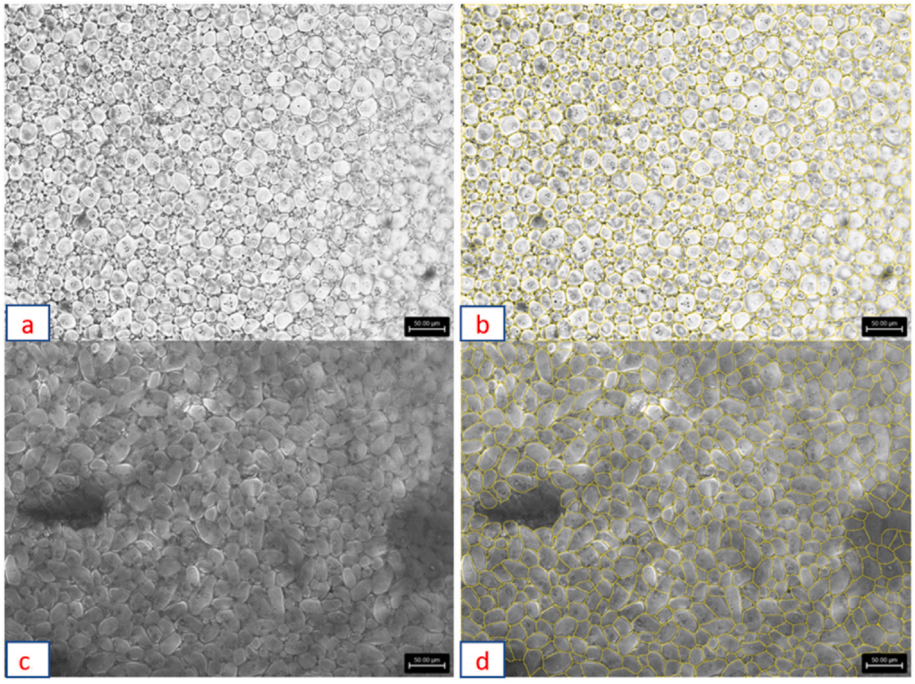

Fig. 1. Microscopic images (a and c) and outlined crystals by Cellpose masking (b and d) taken after 30 min at −8 °C for peptide sample 1 (a and b) and peptide sample 2 (c and d).

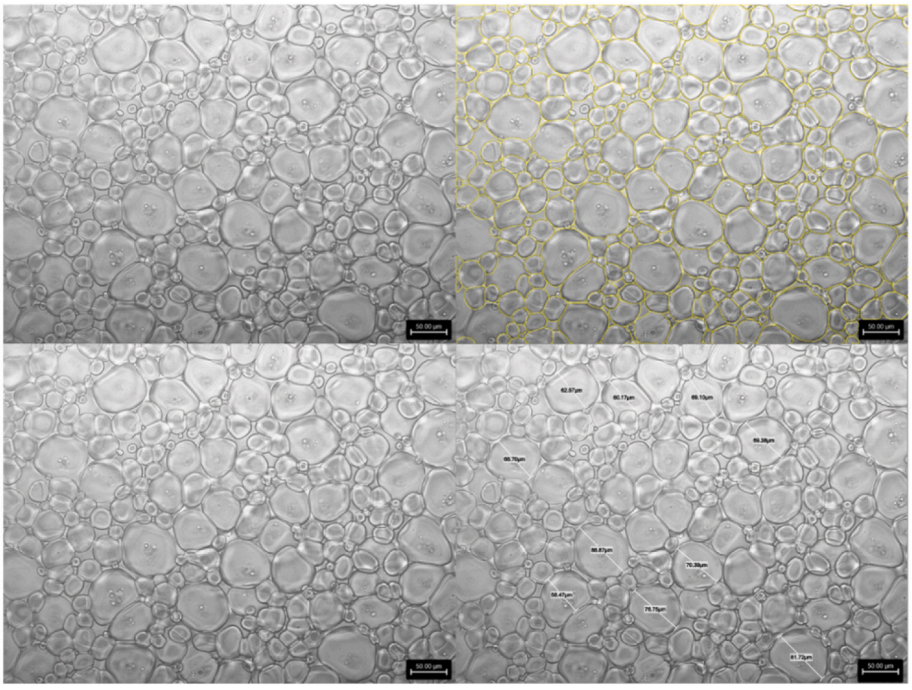

Fig. 2. Images and generated outlines from Cellpose masking (top) and MLGS analysis (bottom) taken after 30 min at −8 °C for peptide sample 3.

crystals generated using both the SA and SSA methods. Evaluated visually, apart from the intentionally unfocused image in Fig. 3 (image c), all images of crystal outlines produced by Cellpose accurately reflect the crystal domains in the corresponding images regardless of size variability seen in Figs. 1a and 2, differing shape seen in Fig. 1c, Fig. 3a, and Fig. 5, and ice crystal density as shown in the SSA (Fig. 5). Fig. 6 shows a gallery of segmented crystals presented in different colors to indicate how the individual ice crystals are recognized.

3.3. Novel automation of ice crystal masking and measurement speed

Automation of ice crystal masking and quantification significantly reduces hands-on time required to assess crystal shape and size. Automation relieves the significant limitation of the MLGS that requires manual measurement of ice crystals. Automated segmentation performed using groups of images is fast, accurate, and less biased than the selection of the largest crystals visually. As shown in Table 2, the time required to mask an entire FOV on our hardware is comparable to the

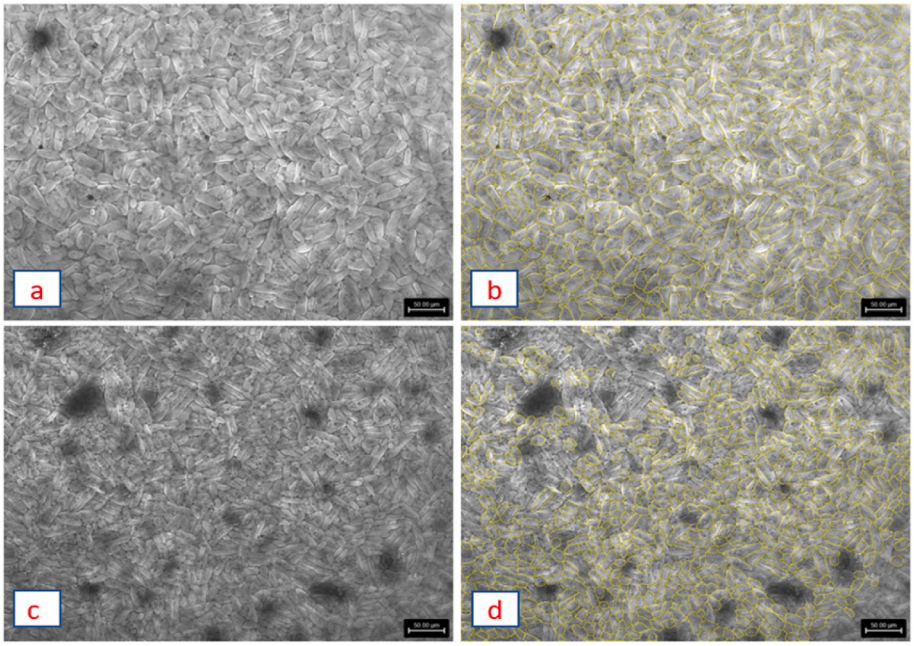

Fig. 3. Pictures of rod-shaped ice crystals with varying image focus produced by a peptide mixture (left, a and c) after 30 min at −8 °C and the masked outline pictures by Cellpose (right b and d). Picture a (and b) was obtained from controlled conditions for image focus and brightness while c (and d) was not controlled prior to masking in Cellpose.

Table 2
Time needed in minutes to mask 10, 20, 50, and 100 images using Cellpose.

Images	Automated time for all images	Automated average time per image	Manual time for all images	Manual average time per image
10	3.94 ± 0.01	0.39	3.35	0.35
20	14.10 ± 0.53	0.71	–	–
50	36.40 ± 2.61	0.73	–	–
100	67.89 ± 0.63	0.68	–	–

Hardware: Dell Precision 3640 Tower Intel® Core™ i7-10700 CPU @ 2.90 GHz, 2904Mhz 8 core processor 16.0 GB of RAM, Intel ® UHD Graphics 630 (n = 3). "–" indicates that data was not collected.

determination of the ten largest crystals and subsequent manual segmentation aided by Fiji. Table 2 shows that when segmenting in bulk, all crystals in an image were masked in a rate of ~70 s per image, on average. The number of crystals present in an FOV has a direct effect on the time to segment, as the group of 10 images contained fewer crystals than the groups of 20, 50, and 100 images, and had a much shorter segmentation time. While segmentation time varies dependent on hardware and the number of crystals present in the FOV, segmentation of images in Cellpose does not require full attention from the user. When there are hundreds of images to analyze for examining IRI agents' concentration effect and dynamic size changes with annealing time, the automated outputs without any fatigue-caused human error or inconsistency is a significant advantage of the new method reported.

3.4. *Factors to consider to ensure accuracy in masking ice crystal domains*

Cellpose's demarcation of crystal domains varied slightly when an image was analyzed under different image brightness, as shown in Fig. 4. Due to the automated detection of ice crystal domains, inadequate picture quality can introduce bias, though not impacting the measurement greatly. Changes in brightness affect the pixel border at which Cellpose identifies crystals, slightly altering crystal diameter output recorded using FD. The FD values of the images, altered only in their brightness, are 25.05 ± 0.00 μm for the dark image, 24.64 ± 0.00

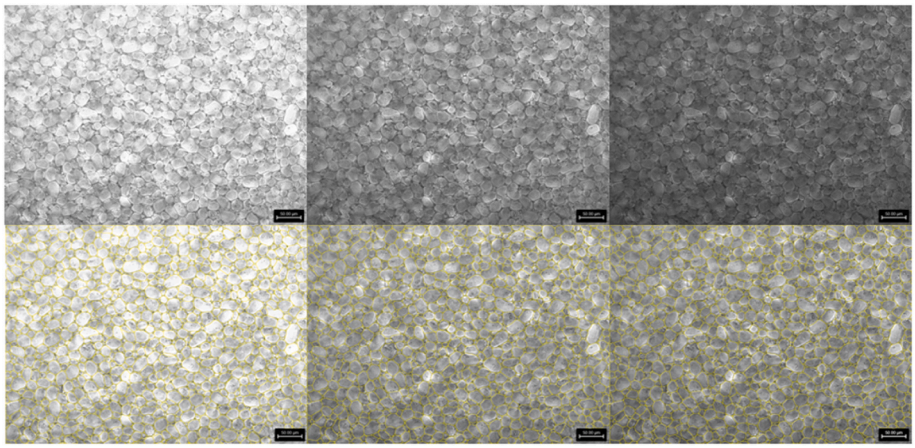

Fig. 4. Images used for reproducibility and effect of light on measurements (Table 2) with both the original image (top) and Cellpose outlined images (bottom).

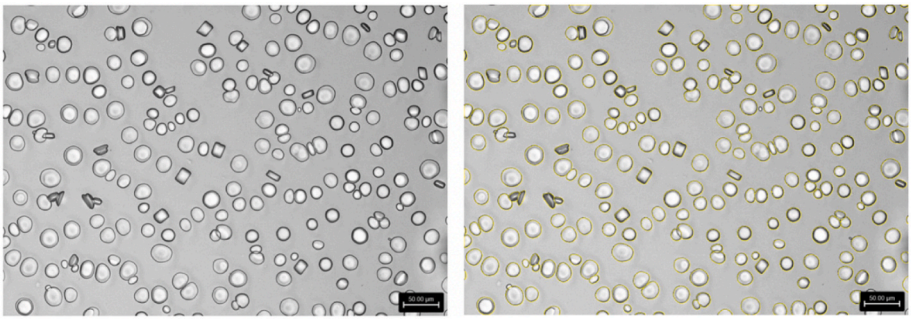

Fig. 5. Sucrose sandwiching images of 4% PEG after annealing (left) and the Cellpose outlined image (right).

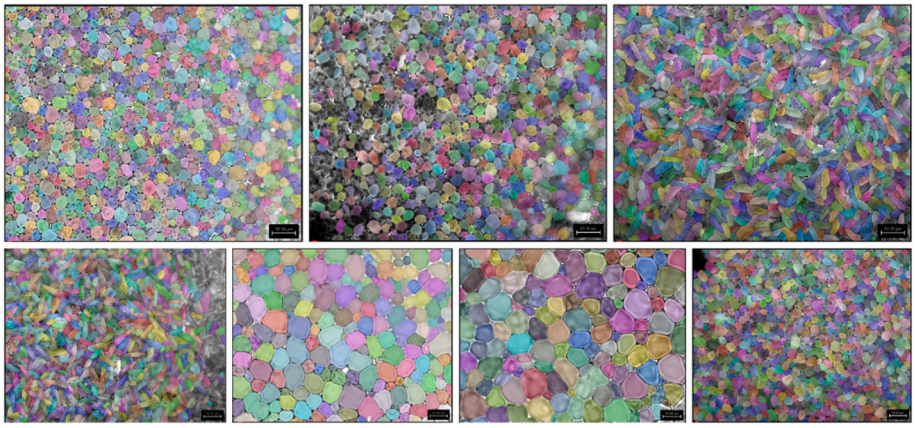

Fig. 6. A gallery of segmented ice crystals presented in different colors to show differentiation of crystals. (For interpretation of the references to color in this figure legend, the reader is referred to the Web version of this article.)

μm for the moderate image, and 23.88 ± 0.00 μm for the bright image. To control for image quality, it is important that images selected for analysis are both in focus and that brightness levels of images are relatively similar. In our case, using a Leica camera and paired software, manipulation of brightness and image sharpness allows optimal imaging of a sample. While Cellpose can successfully mask a wide range of crystal shapes including elongated crystals as shown in Fig. 3, the lack of focus and obvious crystal outlines in Fig. 3c leads to poor outcomes. To maintain image integrity and accurate determination of crystal domains, images should be processed in similar manners prior to masking. The accuracy of the domain recognition ability of Cellpose has previously been evaluated against expert manual demarcation of myofibers investigated by Waisman et al. [15] with similar images to ice crystals formed in the SA. The results obtained show that Cellpose was just as accurate as visual demarcation upon pixel erosion, providing confidence in Cellpose's ability to accurately mask ice crystals when imaging conditions are controlled [15].

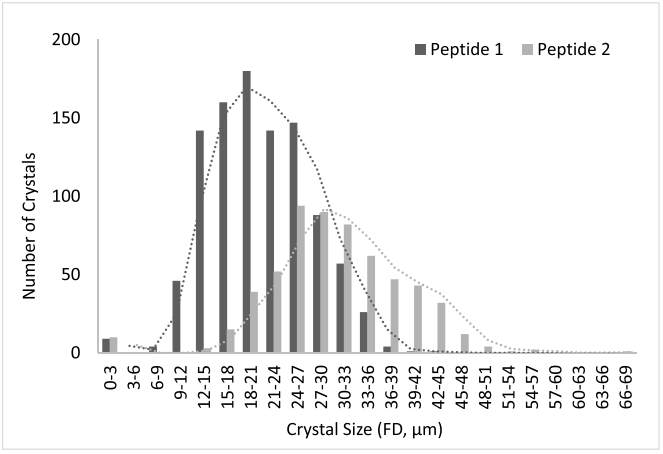

Fig. 7. Ice crystal distribution profile for peptide samples 1 and 2.

3.5. Particle size distribution analysis

Population measurement using Cellpose allows for presentation of particle size distribution analysis. These plots, as shown in Fig. 7, serve as a visual comparisons of ice crystal populations. They not only highlight the differences in crystal size reduction by IRI agents but also provide further information about the ability of an analyte to reduce crystal size uniformly or selectively, as demonstrated by peptide 1 and 2's IRI activity and size uniformity. Unattainable using the MLGS measurement, the ability to plot ice crystal size distributions allow for visualization of IRI activity, assisting the characterization and comparisons of analytes when using other parameters accessible by Cellpose and Fiji, such as the FD and standard deviation.

3.6. Analysis of SSA generated crystals and novel shape descriptors

The SSA method is suitable for obtaining specific information about an analyte. It focuses on isolated crystal shape to understand an IRI active compound's binding plane to the ice crystals [1]. The new automated method of ice crystal segmentation and quantification was used to analyze the SSA images whose crystal shapes differ from Cellpose's training background. Our analysis showed consistent segmentation of ice crystals regardless of differences in shape created in the SSA. Cellpose is shown to be capable of accurately masking these abnormal shapes as shown in Fig. 5. In Fiji, a set of parameters known as "shape descriptors", can be obtained which includes circularity that is more

relevant to the SSA method. A circularity value of 1.0 is representative of a perfect circle, while a value of 0 represents an infinitely elongated polygon [12]. Using Cellpose and Fiji, quantitative data output through measurement of FD and circularity were obtained as 21.30 ± 4.39 μm and 0.86 ± 0.08, respectively. Water or standard buffers form circular crystal disks in the SSA, while ice binding analytes change the morphology of the crystals [3]. Thus, circularity may be used to evaluate ice binding ability. These values can support the largely qualitative analysis used for assessing an analyte's binding characteristics.

3.7. Fiji quantitative data output selection to best evaluate ice crystal size

While particle size analysis using Fiji is common, importation of automatically masked images from the SA provides new quantitative parameters for evaluating ice crystal size that are not commonly seen. Imported in bulk through the LabelstoROIs plugin, relevant parameters available for characterization include FD (max and min), area, and perimeter. While not limited to these parameters, we identified these as the most suitable to characterize ice crystal shape, accounting for irregular particle size. Identified by Briguet et al. [4], FD was presented as the most applicable measurement for analysis of muscle fiber size, relating closely to ice crystal shape and size generated by the SA. Having the lowest coefficient of variation [4], FD was determined to serve as a reliable parameter for measurement of muscle fibers. While Fiji permits the analysis of crystal size using a multitude of parameters, we have adopted measurement of ice crystal diameter using the maximum FD, slightly biasing the measurement for lower IRI activity, but controlled by measuring PEG (negative control, as shown in Fig. 8) using identical parameters. The selection of FD maximum over FD minimum was to align our measurement to the larger crystal size measured by the MLGS approach. FD is more suitable for analyzing irregular particles when compared to the MLGS measurement that uses a consistent angle in the FOV. The maximum or minimum caliper used by the FD measurement accounts for shape inconsistency influenced by an analyte or concentration evaluated, while the MLGS measurement can become biased by the crystal domain due to selection of a fixed angle within the FOV.

3.8. Adoption of Cellpose for measuring ice crystal size and shape

Inspected visually, Cellpose generated masked images were determined to be accurate in demarcation of ice crystals present in the SA and SSA generated images. We determined this by viewing Cellpose produced segmented images overlaid over original, unmodified crystal images, monitoring how closely the segmented crystals matched the original crystal outlines, as shown in Fig. 1b and d. In our experience utilizing Cellpose over twelve months to determine ice crystals boundaries, we have had continuous accuracy in a diverse and wide variety of analytes that affect crystal size and shape.

3.9. Limitations of various methods in ice crystal size quantification

The MLGS measurement most frequently reported in literature was used to quantify ice crystal growth in the SA and SSA. Because it measures the 10 largest ice crystals in an image FOV by the diameter of a consistent angle or ellipsis [2], this measurement presents several limitations in how ice crystals are described quantitatively. If the shape of the ice crystals in a FOV varies greatly, the measurement will be biased [7]. When the selected fixed angle of the MLGS measurement does not correspond to the longest diameter of the crystal because these particles are irregularly shaped and randomly positioned in the FOV, the measurement will not be accurate. If the crystals are visually similarly sized, it will be difficult to differentiate the largest crystals in the FOV. When the sample FOV has a wide distribution of crystal sizes, the ten largest may not be suitable for the characterization of the sample in a holistic sense, thus preventing valid comparisons among samples [7]. These problems intrinsic in the MLGS measurement led to problematic determination of ice crystal size, with quantitative results not consistent with the qualitative assessment of an image.

Aside from the MLGS measurement, a measurement known as the mean grain size (MGS) is also reported in literature, although less frequently. The MGS measures ice crystals in an image FOV by the diameter of a consistent angle and measures every crystal present in the FOV [2]. More commonly reported as the output of the SSA because of the presence of lower numbers of ice crystals in the FOV, the MGS measurement does not have the biased sampling issue. This measurement provides size distribution, but still suffers the problem of not accounting for the irregular shape of the ice crystals. While the MGS serves as the superior measurement when compared to the MLGS, it is less reported in literature likely because of the inconvenience of measuring all crystals. While these measurements can be aided by Fiji, without automated image analysis software, analysis of even a single analyte becomes extremely labor intensive, exacerbated by the hundreds of crystals per image the SA method can generate.

Cellpose for size and shape quantification may also have some limitations. Due to the restricted view of the masking process when running Cellpose with multiple images, verification of the masked crystals cannot be seen prior to importation into Fiji. As a result, manual inspection of crystal outlines generated by Fiji should be performed to ensure the highest accuracy of the masking process before performing treatment comparisons. In the case of misidentified crystal outlines, we recommend using Fiji's function to remove or re-draw masks to ensure data accuracy. Though rare, extreme departures of crystals shape generated by the SA may cause misidentification of crystal domains by Cellpose. In these cases, it may be more beneficial to run Cellpose from the user interface as opposed to segmenting the images in bulk. The additional utility of the user interface to select how close particle shapes match the Cellpose training sets can allow for more accurate segmentation. If manipulation inside the user interface of Cellpose is not sufficient to allow masking of unknown crystal boundaries, the MLGS

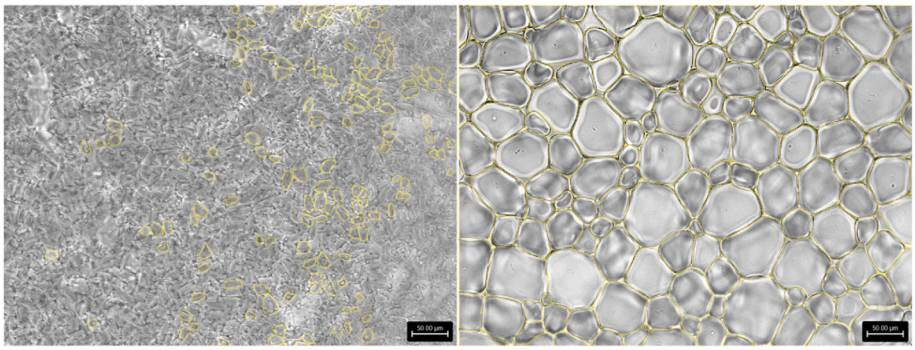

Fig. 8. Images with generated outlines from Cellpose of 0.0125% PVA (left) and 4% PEG (right).

measurement may be applicable to quantify such samples. The pre-trained masks struggled to identify ice crystals by PVA treatment that is commonly used as the positive control for IRI screening, as shown in Fig. 8, because the high IRI activity and extreme recrystallization inhibition lead to an insufficient size for mask overlay. This shortfall of the Cellpose system when used for the evaluation of IRI activity, does not hinder qualitative assessment. When Cellpose is unable to recognize the domain of exceptionally small crystals, the sample is determined to be exceedingly active, and other method of quantification and comparison should be used.

3.10. Expanded application beyond the SA and SSA

The implementation of Cellpose for measurement of ice crystal domains provides a novel method of ice crystal quantification. Cellpose has proved to be extremely useful outside of cellular biological imaging, as demonstrated by this study. This method can likely be adopted for other assays requiring the measurement of ice, other crystals structures or particles viewed under a microscope, such as crystallization of lipids or other particles that have similarities to cellular components or ice crystals.

3.11. Summary of findings and impact

We have fully demonstrated the automated segmentation and quantification method utilizing Cellpose and Fiji to characterize ice crystal size and shape. Our method is adaptable to both the SA and SSA methods that are most widely used in the evaluation of IRI activity. It provides new analytical parameters, has reduced labor input through rapid automation, and provides a more statistically robust output by characterizing all ice crystals in an image FOV. The ability of Cellpose to recognize a host of diverse crystal shapes and sizes allows for easy adoption of this method in measuring a vast number of analytes that can influence ice crystal formation and growth. Our analysis indicates that when expressed in FD, Cellpose and Fiji provide a superior, more holistic analysis of ice crystal size generated by common IRI assays. Our results highlight the consistency and versatility of the method compared to the commonly used MLGS measurement. We expect this analysis method will facilitate a more quantitative and accurate analysis of ice crystals, consequently aiding the discovery of compounds possessing IRI ability to enable long-term freezing storage of foods and biomedical materials.

Funding

This work was supported by the National Science Foundation through funding (award number 2103558) and Hatch/Multi-state project (accession number: 1023982).

Declaration of competing interest

None.

Acknowledgement

N/A.

References

[1] A.A. Ampaw, A. Sibthorpe, R.N. Ben, Use of ice recrystallization inhibition assays to screen for compounds that inhibit ice recrystallization, in: W.F. Wolkers, H. Oldenhof (Eds.), Cryopreservation and Freeze-Drying Protocols, Springer US, New York, NY, 2021, pp. 271–283, https://doi.org/10.1007/978-1-0716-0783-1_9.

[2] C.I. Biggs, C. Stubbs, B. Graham, A.E.R. Fayter, M. Hasan, M.I. Gibson, Mimicking the ice recrystallization activity of biological antifreezes. When is a new polymer "active, Macromol. Biosci. 19 (2019), e1900082, https://doi.org/10.1002/mabi.201900082.

[3] M. Bredow, V.K. Walker, Ice-binding proteins in plants, Front. Plant Sci. 8 (2017), https://doi.org/10.3389/fpls.2017.02153.

[4] A. Briguet, I. Courdier-Fruh, M. Foster, T. Meier, J.P. Magyar, Histological parameters for the quantitative assessment of muscular dystrophy in the mdx-mouse, Neuromuscul. Disord. 14 (2004) 675–682, https://doi.org/10.1016/j.nmd.2004.06.008.

[5] C. Budke, A. Dreyer, J. Jaeger, K. Gimpel, T. Berkemeier, A.S. Bonin, L. Nagel, C. Plattner, A.L. DeVries, N. Sewald, T. Koop, Quantitative efficacy classification of ice recrystallization inhibition agents, Cryst. Growth Des. 14 (2014) 4285–4294, https://doi.org/10.1021/cg5003308.

[6] S. Damodaran, Inhibition of ice crystal growth in ice cream mix by gelatin hydrolysate, J. Agric. Food Chem. 55 (2007) 10918–10923, https://doi.org/10.1021/jf0724670.

[7] J. Jackman, M. Noestheden, D. Moffat, J.P. Pezacki, S. Findlay, R.N. Ben, Assessing antifreeze activity of AFGP 8 using domain recognition software, Biochem. Biophys. Res. Commun. 354 (2007) 340–344, https://doi.org/10.1016/j.bbrc.2006.12.225.

[8] C.A. Knight, J. Hallett, A.L. DeVries, Solute effects on ice recrystallization: an assessment technique, Cryobiology 25 (1988) 55–60, https://doi.org/10.1016/0011-2240(88)90020-x.

[9] F. Kromp, L. Fischer, E. Bozsaky, I.M. Ambros, W. Dorr, K. Beiske, P.F. Ambros, A. Hanbury, S. Taschner-Mandl, Evaluation of deep learning architectures for complex immunofluorescence nuclear image segmentation, IEEE Trans. Med. Imag. 40 (2021) 1934–1949, https://doi.org/10.1109/TMI.2021.3069558.

[10] M. Li, C.R. Luckett, T. Wu, Potent time-dependent ice recrystallization inhibition activity of cellulose nanocrystals in sucrose solutions, Biomacromolecules 23 (2022) 497–504, https://doi.org/10.1021/acs.biomac.1c01201.

[11] A. Rahman, T. Arai, A. Yamauchi, A. Miura, H. Kondo, Y. Ohyama, S. Tsuda, Ice recrystallization is strongly inhibited when antifreeze proteins bind to multiple ice planes, Sci. Rep. 9 (2019) 2212, https://doi.org/10.1038/s41598-018-36546-2.

[12] J. Schindelin, I. Arganda-Carreras, E. Frise, V. Kaynig, M. Longair, T. Pietzsch, S. Preibisch, C. Rueden, S. Saalfeld, B. Schmid, J.Y. Tinevez, D.J. White, V. Hartenstein, K. Eliceiri, P. Tomancak, A. Cardona, Fiji: an open-source platform for biological-image analysis, Nat. Methods 9 (2012) 676–682, https://doi.org/10.1038/nmeth.2019.

[13] C. Stringer, T. Wang, M. Michaelos, M. Pachitariu, Cellpose: a generalist algorithm for cellular segmentation, Nat. Methods 18 (2021) 100–106, https://doi.org/10.1038/s41592-020-01018-x.

[14] I.K. Voets, From ice-binding proteins to bio-inspired antifreeze materials, Soft Matter 13 (2017) 4808–4823, https://doi.org/10.1039/C6SM02867E.

[15] A. Waisman, A.M. Norris, M. Elías Costa, D. Kopinke, Automatic and unbiased segmentation and quantification of myofibers in skeletal muscle, Sci. Rep. 11 (2021), 11793, https://doi.org/10.1038/s41598-021-91191-6.

[16] D. Wang, L.S. Fan, 2 - particle characterization and behavior relevant to fluidized bed combustion and gasification systems, in: F. Scala (Ed.), Fluidized Bed Technologies for Near-Zero Emission Combustion and Gasification, Woodhead Publishing, 2013, pp. 42–76.